View metadata, citation and similar papers at core.ac.uk
brought to you by CORE
provided by Digital.CSIC

Influence of substrate composition on corrosion protection of sol-gel thin films on magnesium alloys in 0.6 M NaCl aqueous solution

A.A. El hadad[1,2], V. Barranco[3], A. Samaniego[1], I. Llorente[1], F.R. García-Galván[1], A. Jiménez-Morales[4], J.C. Galván[1], S. Feliu Jr.[1]

[1]Centro Nacional de Investigaciones Metalúrgicas (CENIM), CSIC, Madrid, Spain.

[2]Physics Department, Faculty of Science, Al-Azhar University, Nasr City 11884, Cairo, Egypt.

[3]Instituto de Ciencia de Materiales de Madrid (ICMM), CSIC, Madrid, Spain.

[4] Universidad Carlos III de Madrid, Departamento de Ciencia e Ingeniería de Materiales e Ingeniería Química, Leganés, Spain.

Corresponding author: Tel.:+34 91 5538900. Fax. +34 91 5347425.
e-mail address: jcgalvan@gmail.com

ABSTRACT

This work researches the protective behaviour of silane based organic-inorganic hybrid coatings on AZ31 and AZ61 magnesium alloy substrates during exposure to 0.6 M NaCl solutions. An attempt is made to determine possible relationships between the degradation of the sol-gel film during its exposure and composition of the metal substrate. Results indicated that the sol-gel coated AZ61 substrate tends to develop corrosion slower than the sol-gel coated AZ31 substrate, tendency that can change by prolonging exposure time. After the curing process, the sol-gel coating formed on the AZ61 substrate is far more perfect, uniform and protective than that which results on the AZ31 substrate, behaviour attributed to the high protective effect of the pre-existing oxide film on the surface of the AZ61 alloy. After several days' immersion, a clear inhibitive effect of the corrosion products formed during the test is observed in the case of the sol-gel coated AZ31, but not with the coated AZ61 alloy substrate, a

phenomenon explained by the carbonate enrichment observed by XPS (X-ray photoelectron spectroscopy).

Keywords: Magnesium alloys, Sol-gel coatings, Electrochemical impedance spectroscopy, X-ray photoelectron spectroscopy, Corrosion properties

1. INTRODUCTION

Magnesium alloys have some advantageous properties as high dimensional stability, low density, high strength, high thermal conductivity, good damping capacity, castability and machinability and they are easily recycled [1]. These alloys show a surface film composed of MgO and $Mg(OH)_2$ which provides corrosion protection in air, but become unstable in aqueous environments [2]. One of the most effective ways to prevent corrosion of metals, is to separate the metallic surface from the corrosive medium by deposition of coating films on the surface [3]. In this case, the coatings protect the substrate by acting as a physical barrier between the metal and its environment [4-10]. Many routes may be followed for the deposition of coatings on metal surfaces, for example, electrochemical deposition, plasma spraying, physical vapor deposition, chemical vapor deposition, and sol–gel technology [11,12].

The sol-gel method enables the obtaining of high reactivity, better purity, avoidance of corrosive by-products, improved control of the product structure, and provides an easy, cost-effective and excellent way to incorporate inorganic compounds into an organic one [13]. The organic-inorganic silane hybrids prepared by sol-gel procedure are of great interest because they combine characteristics of both organics and inorganics [13]. Such coatings display good method for the corrosion protection of metal surfaces including magnesium ones [14-19].

Generally, for an efficient coating, a good adhesion between the metal surface and the deposited film, absence of cracks, are required [20]. In this context, the organic-inorganic silane hybrid with a long alkyl chain may satisfy many of these needs. Silanol

groups (arising from hydrolysis of alkoxy group) can easily react with the hydroxylated magnesium surface, during curing of the silane layer forming covalent bonded metal/film interface (MeOSi) [21]. This increases the adherence of the silanes to the metallic substrates which is considered essential for corrosion protection purposes [21]. Heating of the coated substrates results in formation of siloxane bond (Si–O–Si) network as a result of condensation of the silanol groups which have not reacted with the metal surface. Such cross linking hinders the penetration of the aggressive agents [22].

The objective of this work is to analyse the behaviour of a silane hybrid sol-gel film designed to be applied onto magnesium alloy surfaces for their corrosion protection. For this, two commercial Mg-alloys with differing wt % Al additions, AZ31 (nominally 3 wt. % Al - 1 wt. % Zn) and AZ61 (nominally 6 wt.% Al - 1 wt.% Zn) are coated with the silane hybrid sol-gel film by dip-coating method. The corrosion protection afforded by the sol-gel thin film is evaluated by means of Electrochemical Impedance Spectroscopy (EIS) and hydrogen evolution measurements when the coated Mg alloys are immersed in 0.6M NaCl aqueous solutions. Moreover, a complete study of the coated Mg surfaces before and after the exposure to the saline solutions is made by XPS.

2. MATERIALS AND METHODS

The chemical compositions of the tested magnesium alloys, AZ31 and AZ61, are listed in Table 1. They were fabricated in wrought condition and supplied in 3 mm thick plates by Magnesium Elecktron Ltd. Test specimens were dry ground with successive grades of silicon carbide abrasive paper from P600 to P2000 followed by finishing with

3 and 1 μm diamond paste, cleaned in water and dried with hot air. Due to the high affinity of magnesium with the atmosphere, an attempt was made to keep the exposure time to the atmosphere to a minimum, of around 1 hour, before the immersion of the specimens.

γ-methacryloxypropyltrimethoxysilane (MAPTMS) (98% from Aldrich), and tetramethoxysilane (TMOS) (98% from Fluka), were used as received. Sols for the coatings were prepared starting from a mixture of 4 mols of MAPTMS and 1 mol of TMOS. Ethanol and water were added with the molar ratio (TMOS+MAP)/water/methanol of 1/3/3 [23,24].

The inorganic-organic hybrid coatings were deposited on the AZ31 and AZ61 by using dip coating technique [25] with a withdrawal speed of 9 cm/min and holding time of 60 s. The coated MAPTMS/TMOS-AZ31and MAPTMS/TMOS-AZ61 alloys were then placed in a furnace for 2 h at 120^{o}C for curing. The rest of MAPTMS/TMOS sol was placed 12 hours at 120^{o}C and crushed to convert it into a powder form.

Thermogravimetric analysis (TGA) was performed to determine the thermal degradation of samples using (SETARAM DTA-TG Setsys Evolution -1750) TGA analyser at heating rate of 10^{o}C/min. about 5 mg of the sample was heated from ambient temperature to 900^{o}C at a heating rate of 20^{o}C/min.

X-ray Diffraction measurements were made on the prepared hybrid using a Siemens D-5000 diffractometer with CuKα monochromatic radiation (λ= 0.15406 nm). The XRD data were collected at a room temperature over the 2θ range of 10°–100° at a step size of 0.02°

The surfaces of the coated substrates was studied by using attenuated total reflectance-infrared spectroscopy (FTIR-ATR) using a Nicolet Magna IR 550 in the range of 400 and 4000 cm^{-1}.

Photoelectron spectra were recorded using a Fisons MT500 spectrometer equipped with a hemispherical electron analyser (CLAM 2) and a Mg Kα X-ray source operated at 300 W. The samples were fixed on small flat discs on a *XYZ* manipulator and placed in the analysis chamber. The residual pressure in this ion-pumped analysis chamber was maintained below 10^{-8} torr while data was being attained. The spectra were collected for 20–90 min depending on the peak intensities, at a pass energy of 20 eV, which is typical for high-resolution conditions. The intensities were estimated by calculating the area under each peak after smoothing and subtraction of the S-shaped background and fitting the experimental curve to a combination of Lorentzian and Gaussian lines of variable proportions. Although specimen charging was observed, it was possible to determine accurate binding energies (BEs) by making references to the adventitious C 1s peak at 285.0 eV. The atomic ratios were calculated from the peak intensity ratios and the reported atomic sensitivity factors [26]. The measurements were performed at take-off angles of 45° with respect to the sample surface. The sampled areas were 1 x 1 mm^2.

Images of the specimen surfaces were obtained in original and polished condition using an atomic-force microscope (AFM). All images (20 x 20 µm) were taken in the 5100 AFM/SPM from Agilent Technologies working in tapping mode using Si type AFM cantilevers with a normal spring constant of 40 N/m and a typical radius of 10 nm from

Applied Nanostructures. Images were acquired at a resolution of 512 x 512 points and subjected to first-order flattening.

The corrosion of the sol-gel coated magnesium alloys was estimated by determining the volume of hydrogen evolved during the corrosion process. Samples for hydrogen gas collection, to characterise corrosion rate during solution immersion, were cut into square coupons with dimensions of 2 cm × 2 cm x 0.3 cm, and vertically immersed in 700 ml of quiescent 0.6M NaCl solution for 11 days in a beaker open to laboratory air at 20 ± 2 °C. All of the specimen surface has been exposed to the corrosion test. The hydrogen evolved during the corrosion experiment was collected in a burette by a funnel above the corroding sample, as described by Song et al [27-29]. All these experiments were run simultaneously and each sample was subjected to essentially the same temperature and exposure history.

Electrochemical impedance measurements were conducted in 0.6 M NaCl aqueous solution during 14 days of immersion at room temperature (25ºC). A Metrohm / Eco Chemie Autolab PGSTAT30 Potentiostat/Galvanostat Electrochemical System equipped with a frequency response analyser FRA2 module was used to carry out these measurements. The frequency ranged from 100 kHz to 1 mHz with 5 points/decade, whereas the amplitude of the sinusoidal potential signal was ±10 mV with respect to the open circuit potential. A conventional three-electrode setup was employed: Ag/AgCl and graphite were used as reference and counter electrodes, respectively, and the material under study was the working electrode. The exposed area of the working electrode was 9 cm^2.

3. RESULTS

The thermal degradation of the MAPTMS/TMOS hybrid was studied using TGA. The TGA curve is shown in Fig 1. From this curve, it is clear that the thermal degradation of the silane hybrid occurs through three mass loss steps namely, Region I, Region II and Region III. In region I the first weight loss, below 350ºC, is attributed to the evaporation of water and condensation by-products [30]. The weight loss in region II, between 350 and 550ºC, is attributed to the burning or combustion of organic compounds in the hybrid [30]. The third weight loss stage region III, above 550ºC, is ascribed to the complete burning of the organics in the hybrid [30]. There is no major weight loss afterwards, indicating that the organic groups have been completely burnt off.

The XRD patterns of, MAPTMS/TMOS deposited on different surfaces of AZ31 and AZ61 alloys (Polished and originals) are showed in Figure 2. All the XRD patterns exhibited a single broad diffused peak typical for an amorphous material. Surely, because silane-based sol–gel chemistry consists primarily of hydrolysis and condensation reactions of alkoxysilane precursors that form amorphous materials as the reactions proceed [31].

The FTIR-ATR spectra of a dip-coated AZ31 and AZ61 alloys is presented in Fig. 3 and the corresponding band assignments for this compound are presented in Table 2. All hybrids present the characteristic asymmetric Si–O–Si stretching vibration, silica network peak around 1010 cm^{-1} which are the structural backbone of the hybrid material [13]. The band at 2942 cm^{-1} may be ascribed to the C-H stretching absorptions of the CH_3 residues. The bands at 1450 cm^{-1} correspond to the symmetrical and asymmetrical CH_3 deformational (umbrella) modes [13]. The

stretching vibration of C=O group at 1750 cm^{-1} is attributed to the carboxyl radical of acrylate [13].The existence of these residues indicates that the film heated to 120^{o}C/2 hours still holds some hydrocarbon content. Therefore, FTIR-ATR confirms the presence of both organic and inorganic structures in the hybrid coatings, i.e. that the coating structure is formed by a silica network of Si–O–Si bonds interrupted in some points by organic groups. The band at 893 cm^{-1} corresponded to Mg–O–Si, which indicated that the cross linking was made between Mg surface and deposited layer.

Figure 4 compares the AFM macro surface morphology of the AZ31 and AZ61 coated specimens. The AFM observation (Fig. 4b) showed the formation of a uniform, homogeneous, crack free and highly adherent, protective film on the substrate that may lead to a good corrosion resistance of the AZ61 alloy coated with the organic–inorganic hybrid coating. Coating flexibility may be a consequence of the high organic content of the coatings which was confirmed by FTIR-ATR analysis. In contrast, porous features and macroscopic defects become apparent in the AFM observations of the sol-gel coated AZ31 substrate (Fig. 4a).

Table 3 shows the elemental composition obtained by XPS on the surface of the sol-gel coating applied to the AZ31 and AZ61 alloy substrates after the curing process. An important carbon, oxygen and silicon contents are observed, which may be related to the presence of the sol-gel coating.

Figure 5 compares the evolution of the Nyquist diagrams obtained for the bare alloys coated with those corresponding to the coated alloys after different stages of testing. With the coated specimens, apparently one single capacitative loop at high

frequencies (HF) is present during the initial stages of testing (Figs 5a and Figs 5e-5g). As immersion time increased, an inductive loop at low frequencies tends to become more or less patent (Figs 5b-5d and 5h).

At the start, the diameter (R_{HF}) of the HF semicircle will mainly depend on the effect of the sol-gel coating but, after a longer immersion, the charge transfer resistance will be influenced by the progressive deterioration and porosity of the coating. Fig. 6 shows the evolution of the charge transfer resistance versus immersion time in the exposure of the alloys to the 0.6 M NaCl solution. Comparing the R_{HF} values for the sol-gel coated specimens with the corresponding reference values for the untreated specimens it is observed the existence of a beneficial effect of the coating, particularly during the initial stages of the corrosion test.

Figure 7 compares the hydrogen evolution data for the sol-gel coated AZ31 alloy substrate with those corresponding to the sol-gel coated AZ61 alloy for 11 days in 0.6M NaCl solution. From Figure 7 it can be deduced that the hydrogen evolution data for the coated AZ31 alloy progresses according to an approximately parabolic law typical of a process that is under control by diffusion, possibly associated with the effect of the precipitation of insoluble and protective magnesium corrosion products on the sol-gel coating.

Two different regimes were observed in the corrosion rate curve of the coated AZ61 alloy: an initial period of low corrosion rate and, after about 3 days, a much less protective effect with a moderately accelerated linear kinetics attributed to the

breakdown of the sol-gel film and activation of microgalvanic corrosion enhanced by the significant β phase fraction in the AZ61 alloy.

Table 4 shows the elemental composition obtained by XPS on the surface of the sol-gel coated alloy AZ31 and AZ61 after immersion for 15 days in 0.6 M NaCl..On the coated AZ31 alloy, attention is drawn to the important increase in the Cl and Na content observed respect to the corresponding coated AZ61 alloys and the presence of a significant silicon content. In contrast to the coated AZ61 alloys, the surface of the coated AZ31 alloy shows a large excess of sodium over its anion (chloride). Probably, because of the higher intensity of the Cl2p peak observed by XPS in the surface of the coated AZ31 alloy after immersion, the effect from its respective chlorine Auger induced peak ($ClKL_1L_{23}$) at a binding energy of 1072.0 eV is a significant increase in the area of the Na1s spectrum. Also, an important increase in the Magnesium and Oxygen content is observed in the coated AZ61 alloys compared with the outer surface of the coated AZ31 alloys.

It is interesting to note that the C1s, O1s, Mg2p and Si 2p high resolution XPS peaks (Figs 8 and 9) seem not to be significantly affected by charging effects and their uncorrected positions agree well with most of the literature data. [32]. On the other hand, charging effects due to the very high amounts of Cl and Na elements deposited on the outer surface of the magnesium alloys after immersion to the saline solution results in a shift of the Cl2p and Na 1s peaks up to 2.0 eV towards a higher binding energy. Therefore, we have referenced the binding energy of the Cl2p (Figure 9b) and Na1s peak (Figure 9c) to the position of Na1s peak in sodium chloride at 1072.4 eV

[33]. Figure 8 compares the high resolution XPS C1s, O1s and Mg 2p spectra obtained coated surfaces AZ61 and AZ31 alloys after 15 days immersion in 0.6M NaCl solution. The C1s spectra obtained on the surface of the coated AZ61 alloy substrate (Figs 8a) can be fitted using three components at different binding energies: at 285.0 eV, which may be associated with the presence of C-C/C-H groups. This component, appears on the surface (<3 nm in thickness) of almost any metal in contact with the atmosphere at room temperature, irrespective of its composition At 286.5 eV appears one component less intense associated to the presence of C-O groups and a very low intensity component at 290 eV associated with the presence of magnesium carbonate [34]. In the spectra obtained on the surface of the coated AZ31 alloys substrate (Fig 8b) the C1 peak splitting at the low binding energy side may be associated to differential charge effects. The component at 285.0 eV may be associated to C-C/C-H groups in the relatively conducting inner corrosion layer next to the metallic substrate and the component at approximately 287 eV may be associated with the presence of similar groups on the more isolating NaCl particles of the outer surface Likewise, a shift of about 2eV is seen in the binding energy, accompanied by an increase in the intensity of the component that appears at the highest binding energies of close to 292.0 eV, which may be attributed to the presence of significant amounts of magnesium carbonate which charges appreciably in contact with the NaCl crystals (non-conducting).

The O1s high resolution spectra obtained on the surface of the sol-gel coated alloy AZ61 after immersion for 15 days (Fig 8c) shows the most intense component at a binding energy of 532.2 eV associated with the presence of oxygen in the form of $Mg(OH)_2$ and another less intense at 533.6 eV which may be attributed to magnesium carbonate [35]. The Mg2p high resolution spectra obtained on the coated AZ61 alloy

may be fitted with two components (Fig. 8d). The first and more intense component at a binding energy of 50.8 eV, which is associated with the presence of magnesium in the form of $Mg(OH)_2$. At 52.6 eV a component of lower intensity is also found, related to magnesium in the form of magnesium carbonate. As was previously observed in the C1s peak (Figs. 8a and 8b), it is important to note the significant increase in the intensity of the component which appears at the highest binding energies (magnesium carbonate) in the O1s and Mg2p spectra observed in the coated AZ31 alloy (Figs 8d and 8f) compared with that of the coated AZ61 alloy (Fig. 8c and 8e).

Fig 9 shows the Si2p (a), Cl 2p (b) and Na1s (c) XPS high resolution spectra on the surface of coated AZ31 alloy after immersion for 15 days. In the Si2p spectrum (Fig.9a) only one component appears that is associated with the presence of silicon in Si-O bonds [36]. The Cl2p high resolution spectrum (Fig. 9b) may be fitted to one doublet with a binding energy of 199.3 eV associated with the presence of Cl^-. Finally, the Na1s spectrum (Fig. 9c) may be fitted to one component at 1072.6 eV associated with the presence of sodium (Na^+) ions [33].

Table 4 compares the atomic percentages of carbonate on the surface of the corrosion layers formed on the AZ31 and AZ61 alloys exposed to the NaCl solution. The atomic percentages of carbonate were obtained from the area of the CO_3^{2-} components used in the fitting of the C1s spectra (Figs. 8a and 8b) and the atomic percentages of C obtained by XPS on the surface of the corrosion layer formed on the AZ31 and AZ61 alloys (Table 4). It is important to note, the significant increase in the amount of carbonates observed by X-ray photoelectron spectroscopy (XPS) on the surface of the coated AZ31 alloy, increased by a factor of around 2, compared with the coated AZ61 alloys.

4. DISCUSSION

4.1. Influence of the composition of Mg-Al alloys substrate on the sol-gel coatings surface morphology.

In the XPS analysis of the external surface of the sol-gel coatings formed on the AZ31 substrate after the curing process, attention is drawn to the detection of significant amounts of magnesium (Table 3) which indicated the significant presence of discontinuities or pores in the coating that leave the substrate surface exposed. In contrast, the absence of magnesium indicates that the surface of the AZ61 alloy substrate is completely covered by the sol-gel coating. In Fig 4a which represents the visual appearance of the sol-gel coatings formed on the AZ31 substrate, one can see that the surface is not uniform, with areas without apparent macroscopic defects coexisting with other areas with visible macroscopic pores or defects. In contrast, the sol-gel coating formed on the AZ61 alloy substrate looks (Fig 4b) far more perfect and uniform. The formation of porous, non-uniform coatings during its deposition has been reported by Song and Liu [37] appearing to be the result of the hydrogen evolution closely associated with the magnesium dissolution from the substrate.

In previous studies [38-40] with the same alloys immersed in a 0.6 M NaCl saline solution, we observed that the native oxide layer formed on the polished AZ61 surface was more protective than that on the AZ31 surface in the early stages of testing. The difference seemed to be due to the strong protective effect of the uniform, passivation film of magnesium oxide that is formed spontaneously on the as-polished surface of the AZ61 magnesium alloy. At the beginning of the sol-gel coating formation, it is likely that this protective and homogeneous surface layer initially present on the polished AZ61 alloy substrate had a greater capability to isolate this alloy from the acqueous

electrolyte environment and the effects of hydrogen evolution compared to the AZ31 alloy, with the result of the growth of a more perfect sol-gel coating than that of the AZ31 alloy.

4.2. Relationship between the surface morphology of the sol-gel coating and their corrosion resistance in saline solutions.

It seems likely that some of the differences that have been revealed in the surface morphology of the sol-gel coatings formed on the AZ31 and AZ61 alloys have an impact on the corrosion behaviour. As commented earlier, the more significant changes that have been observed on the surface of the sol-gel coating, is the presence of macroscopic defects or pores as result of the interactions between coating and substrate during curing.

After less than 1 day of exposure, EIS measurements have revealed a significant reduction in the impedance values of the coated AZ31 alloy substrate compared with those observed at the start of exposure, reaching similar values to the same alloy in bare state (Fig. 6a). The presence of macroscopic defects or pores in the coating formed on the AZ31 alloy (Fig 4a) had the effect of decreasing its barrier properties, being lost any relevant influence on corrosion protection

In contrast to the findings with the AZ31 alloy, the sol-gel coating significantly improves the corrosion resistance of the AZ61 alloy as observed in the R_{HF} values obtained in the coated AZ61 specimens, clearly exceeding the bare substrate values during the first seven days of corrosion testing in presence of the highly aggressive 0.6M NaCl solution (Fig. 6b). It seems likely that the uniformity and the absence of visible defects

on the sol-gel coating formed on the AZ61 slow down the corrosion process by physically blocking the active sites on the metal surface (i.e., presence of β- phase) diminishing the rate at which Cl^- ions are transported through the sol-gel coating.

4.3. Influence of the composition of corrosion products on the sol-gel coating corrosion resistance in saline solutions.

After 7 days of immersion and until the end of the test, low Rt values were obtained from the sol-gel coated AZ61 alloy (Fig. 6b); values that differ relatively little from those obtained with the bare alloy, indicating that the sol-gel coating in such circumstances does not prevent significantly the corrosion. Unlike the AZ61 alloy, an important increase of the R_{HF} values with time of exposure to the aggressive medium is observed on the sol-gel coated AZ31 alloy after 7 days of exposure (Fig. 6a).

It seems likely that some of the differences on corrosion behaviour of the tested specimens obey to differences in the chemical composition observed on the surface of the specimens during exposure to the saline solution. In the sol-gel coated AZ31 alloy the clear tendency for R_{HF} to increase and, therefore, corrosion rate to decrease with immersion time (Fig. 6a) suggests a reinforcement of the protective action of the film associated with the formation and accumulation of insoluble corrosion products at the base of pores of the coating. In this alloy, XPS analysis has revealed an appreciable content of magnesium carbonate, suggesting a positive effect of these species on the corrosion resistance, result in line with the protective role of the carbonate products observed by Wang et al [41] after immersion of AZ31 and AZ91 magnesium alloys in diluted (0.01M) NaCl solution.

However, in our work, remarkably high values of corrosion rate are deduced from Fig. 6b for the AZ61 alloy after several days of corrosion test, and the XPS analysis reveals the presence of $Mg(OH)_2$ as the major component of the corrosion product layer. Therefore, these corrosion products do not appear to provide effective protection to the AZ61 alloy against the much more concentrated 0.6M NaCl solution used here.

The differences observed between the contents of magnesium hydroxide and carbonate precipitated on the surface of the two sol-gel coated alloys suggests differences in the pH of the solution close to the surface of the coated substrate during the corrosion test. In the coated AZ61 alloy, the presence of β-phase and micro-galvanic couples along the grain boundaries of the matrix of magnesium (α phase) increases the magnesium dissolution and production of OH^- ions from the cathodic reaction favoring the formation of hydroxide by means of a precipitation reaction. In the case of the coated AZ31 alloy, the practically nil presence of β-phase contributes to a significant decrease in the magnesium dissolution rate and pH. Wang et al have mentioned [42] the greater stability of the MgCO3 compared to Mg(OH)2 on diminishing the pH of the solution. As a consequence, it is hypothesized that the lower pH on the surface of the coated AZ31 alloy during immersion helps the formation of greater amounts of carbonate.

CONCLUSIONS

1) AFM observations and XPS analysis revealed that the sol-gel coatings formed on the surface of AZ61 alloy are far more perfect, uniform and free from macroscopic defects than those formed on the AZ31 alloy. This behaviour is attributed to the effect of the native oxide film initially present on the surface of the AZ61 alloy, which inhibits

the attack of magnesium. However, with the AZ31 alloy, the native oxide film is not sufficiently protective to prevent some magnesium dissolution and associated hydrogen evolution, causing macroscopic pores during the curing process of the sol-gel film formation.

(2) Probably due to the effects of a defective coating, in the first 24 hours of corrosion test EIS measurements showed corrosion rates for the sol-gel coated AZ31 alloy about ten times higher than for the AZ61 alloy with a better barrier effect.

(3) After about six days of immersion in 0.6 M NaCl solution, there is a gradual reduction of the corrosion rate with time in the case of the sol-gel coated AZ31 alloy, phenomenon attributed to the accumulation of corrosion products on the corroding surface. This effect is not shown in the AZ61 alloy, and suggests the existence of a strong link between carbonate enrichment observed by XPS and corrosion resistance of the treated surfaces.

4) The best corrosion resistance was obtained with the sol-gel coated AZ61 alloy at the initial (first week) immersion time in the 0.6 M NaCl solution. Less relevant were the results obtained initially with the sol-gel coated AZ31 alloy.

In the AZ61 alloy, the weakening of the barrier effect with immersion time facilitates the initiation of a process of accelerated microgalvanic corrosion, process which is not possible in the AZ31 alloy. For this reason, in the long term, AZ31 alloy may show eventually better overall results. .

ACKNOWLEDGEMENTS

The authors express their gratitude to Prof. S. Feliu for several clarifying and stimulating discussions during the course of this work. They also gratefully acknowledge financial support for this work from the Ministry of Economy and Competitivity of Spain (MAT 2009-13530 and MAT2012-30854). A.A. El Hadad acknowledges a pre-doctoral contract JAE financed by CSIC. V.B. acknowledges a Ramon y Cajal researcher contract financed by CSIC and MINECO.

References

[1] J. Zhang, Z. Zhang, Magnesium alloys and their applications, Chemical Industry Press of China, Beijing, 2004.

[2] T.T. Hu, B. Xiang, S.G. Liao, W.Z. Huang, Anti-Corros. Methods Mater. 57 (2010) 244-248.

[3] H. Altun, H. Sinici, Mater. Charact. 59 (2008) 266-270.

[4] H. Leidheiser Jr., Corrosion 38 (1982) 374-383.

[5] S. Feliu, J.C. Galván, M. Morcillo, Corros. Sci. 30 (1990) 989-998.

[6] G. Grundmeier, W. Schmidt, M. Stratmann, Electrochim. Acta 45 (15-16) (2000) 2515-2533.

[7] J.E. Gray, B. Luan, J. Alloy. Compd. 336 (1-2) (2002) 88-113.

[8] V. Barranco, S. Feliu Jr., S. Feliu, Corr. Sci. 4 (2004) 2221-2240.

[9] M. García-Heras, A. Jiménez-Morales, B. Casal, J.C. Galván, S. Radzki, M.A. Villegas, J. Alloy. Compd. 380 (2004) 219-224.

[10] D. Wang, G.R.Bierwagen, Prog. Org. Coat. 64 (2009) 327-338.

[11] C.J. Brinker, A.J. Hurd, P.R. Schunk, G.C. Frye, C.S. Ashley, J. Non-Cryst. Solids. 147 (1992) 424-436.

[12] J.D.Wright, N.A.J. Sommerdijk, Sol–Gel Materials Chemistry and Applications, CRC Press, OPA Overseas Publishers Association, 2000.

[13] A.A. El Hadad, D. Carbonell, V. Barranco, A. Jiménez-Morales, B. Casal, J.C. Galván, Colloid. Polym. Sci. 289 (2011) 1875-1883.

[14] A.L.K. Tana, A.M. Soutar, I.F. Annergren, Y.N. Liu, Surf. Coat. Technol. 198 (1-3) (2005) 478-482.

[15] J.Y. Hu, Q. Li, X.K. Zhong, W. Kang, Prog. Org. Coat. 63 (1) (2008) 13-17.

[16] S.V. Lamaka, M.F. Montemor, A.F. Galio, M.L. Zheludkevich, C. Trindade, L.F. Dick, M.G.S. Ferreira, Electrochim. Acta 53 (14) (2008) 4773-4783.

[17] V. Barranco, N. Carmona, J.C. Galván, M. Grobelny, L. Kwiatowski, Prog. Org. Coat. 68 (2010) 347-355.

[18] R.G. Hu, S. Zhang, Su; J.F. Bu, C.J. Lin, G.L.Song, Prog. Org. Coat.73 (2-3) (2012) 129-141.

[19] F. Brusciotti, D.V. Snihirova, H. Xue, M.F Montemor, S.V. Lamaka, M.G.S. Ferreira, Corros. Sci. 67 (2013) 82-90.

[20] R. Viana, A.R. Machado, J. Braz. Soc. Mech. Sci. Eng. 31 (2009) 327-332.

[21] E.P. Plueddemann, Silane Coupling Agents, (2nd ed), Plenum Press, New York, 1991.

[22] I. Graeve, J. Vereecken, A. Franquet, T. Van Schaftinghen, H. Terryn, Prog. Org. Coat. 59 (2007) 224-229.

[23] A. Jiménez-Morales, J.C. Galván, P. Aranda, E. Ruiz-Hitzky, Mater. Res. Soc. Symp. Proc.519 (1998) 211-216.

[24] A. Jiménez-Morales, J.C. Galván, P. Aranda, Electrochim. Acta, 47 (13-14), (2002) 2281-2287.

[25] A.A. El Hadad, V. Barranco, A. Jiménez-Morales, E. Peón, J.C. Galván, J. Phys. Conf. Ser. 252 (2010) 012007.

[26] C.D. Wagner, L.E. Davis, M. V. Zeller, J.A. Taylor, R.H. Raymond, L.H. Gale, Surf. Interface Anal. 3 (1981) 211-225.

[27] G.L. Song, A. Atrens, D. Stjohn, J. Naim, Y. Li, Corros. Sci. 39 (1997) 855-875.

[28] G.L. Song, A. Atrens, X.L. Wu, B. Zhang, Corros. Sci. 40 (1998) 1769-1791

[29] G.L. Song, A. Atrens, M. Dargusch, Corros. Sci. 41 (1998) 249-273.

[30] H.Y. Park, D.P. Kang, M. K. Na, H. W. Lee, H. H. Lee, D. S. Shin, J Electroceram. 22 (2009) 309–314.

[31] G. Frenzer, W.F. Maier, Annu. Rev. Mater. Sci. 36 (2006) 281-331.

[32] M. Liu, S. Zanna, H. Ardelean, I. Frateur, P. Schmutz, G.L. Song, A. Atrens, P. Marcus, Corros. Sci. 51 (2009) 1115-1127.

[33] J. F. Watts, J.E. Castle, J. Mater. Sci. 19 (1984) 2259-2272.

[34] H.B. Yao, Y.Li, A.T.S. Wee, Appl. Surf. Sci. 158 (2000) 112-119.

[35] N.C. Hosking, M.A. Ström, P.H. Shipway, Corros. Sci. 49 (2007) 3669-3695.

[36] V.H.V. Sarmento, M.G. Schiavetto, P. Hammer, A.V. Benedetti, C.S. Fugivara, P.H. Suegama, S.H. Pulcinelli, C.V. Santilli, Surf. Coat. Technol. 204 (2010) 2689-2071.

[37] G.L. Song, M.H. Liu, Corros. Sci. 53 (2011) 3500-3508.

[38] S. Feliu Jr., C. Maffiotte, A. Samaniego, J.C. Galván, V. Barranco, Electrochim. Acta 56 (2011) 4554-4565.

[38] A. Samaniego, I. Llorente, S. Feliu Jr, Corros. Sci. 68 (2013) 66–71.

[40] S. Feliu Jr, C. Maffiotte, A. Samaniego, J. C. Galván, V. Barranco, Appl. Surf. Sci. 257 (2011) 8558–8568.

[41] L. Wang, T. Shinohara, B.P. Zhang, Appl. Surf. Sci. 256 (2010) 5807-5812.

[42] L. Wang, T. Shinohara, B.P. Zhang, J. Alloys Compd. 496 (2010) 500-507.

FIGURE CAPTIONS

Figure 1. TG trace of the prepared MAPTMS/TMOS hybrids.

Figure 2. Powder XRD patterns of MAPTMS/TMOS hybrid deposited on different surfaces of AZ31 and AZ61 alloys (Polished and originals).

Figure 3. Representative FTIR-ATR absorption spectra of the prepared MAPTMS/TMOS Hybrid / Mg Alloys.

Figure 4. AFM surface morphologies of the sol-gel coating formed on the AZ31 (a) and AZ61 (b) alloys substrates.

Figure 5. Variation in Nyquist plot as a function of the coated alloy type substrate over 14 days immersion in 0.6M NaCl solution.

Figure 6. Variation in R_{HF} values as a function of the coated alloy type substrate over 14 days immersion in 0.6M NaCl solution.

Figure 7. Hydrogen evolution curves as a function of the coated alloy type substrate over 11 days immersion in 0.6M NaCl solution.

Figure 8. C1s, O1s and Mg2p high-resolution peaks obtained by XPS on the surface of the sol-gel coated as a function of the type alloy substrate after 14 days immersion in 0.6M NaCl solution.

Figure 9. Si2p (a), Cl 2p (b) and Na1s (c) high-resolution peaks obtained by XPS on the surface of the sol-gel coated AZ31 alloy substrate after immersion in 0.6 M NaCl solution for 14 days.

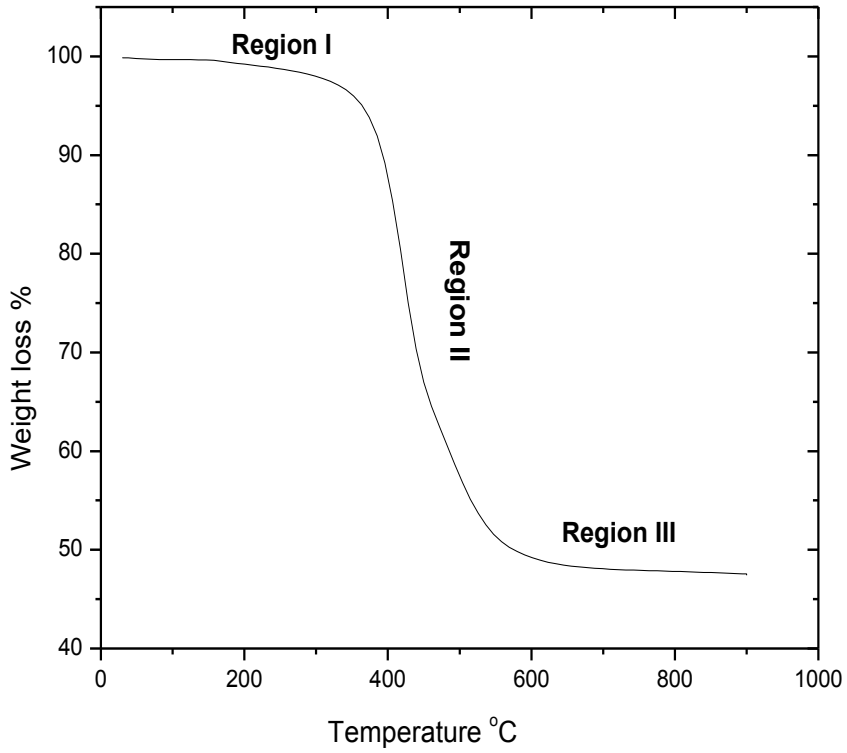

Figure 1. TG trace of the prepared MAPTMS/TMOS hybrids

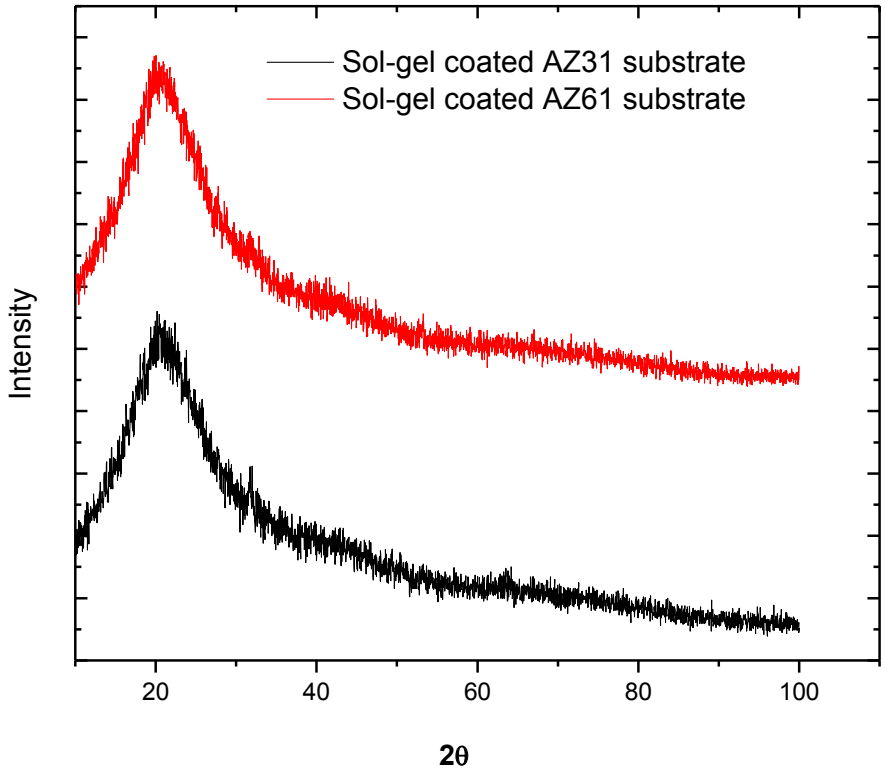

Figure 2. Powder XRD patterns of MAPTMS/TMOS hybrid deposited on different surfaces of AZ31 and AZ61 alloys (polished and originals)

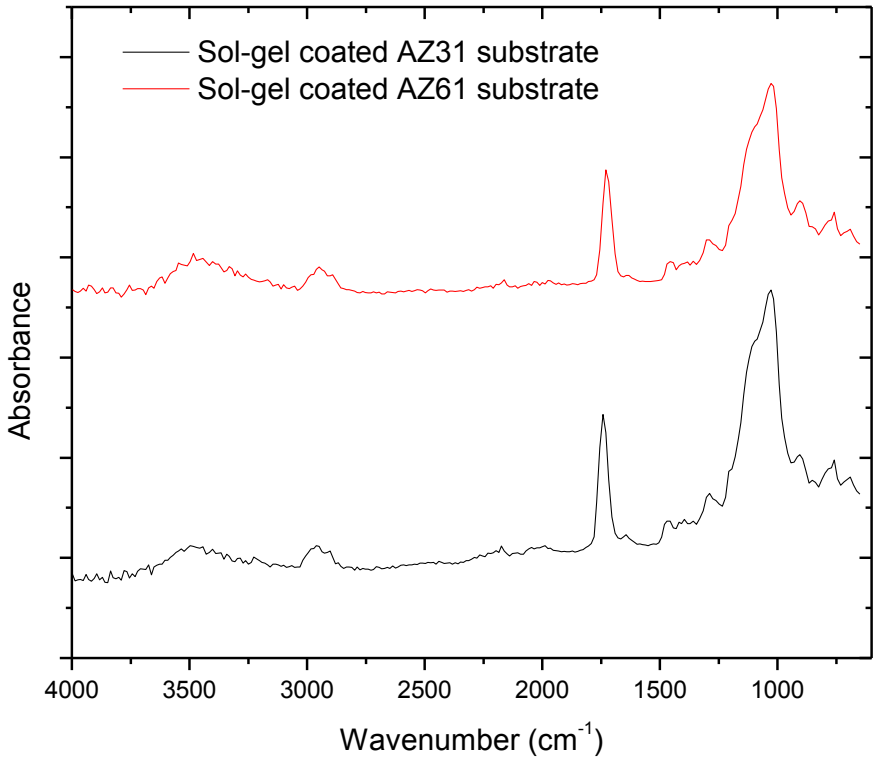

Figure 3. Representative FTIR-ATR absorption spectra of the prepared MAPTMS/TMOS Hybrid / Mg Alloys

Sol-gel coated
AZ31 substrate

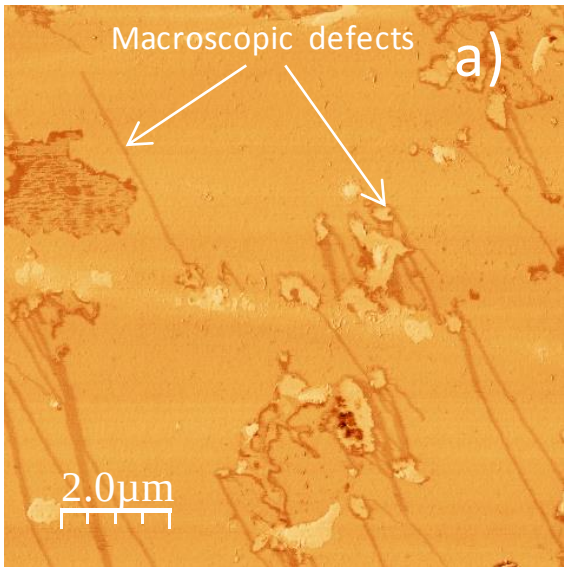

Sol-gel coated
AZ61 substrate

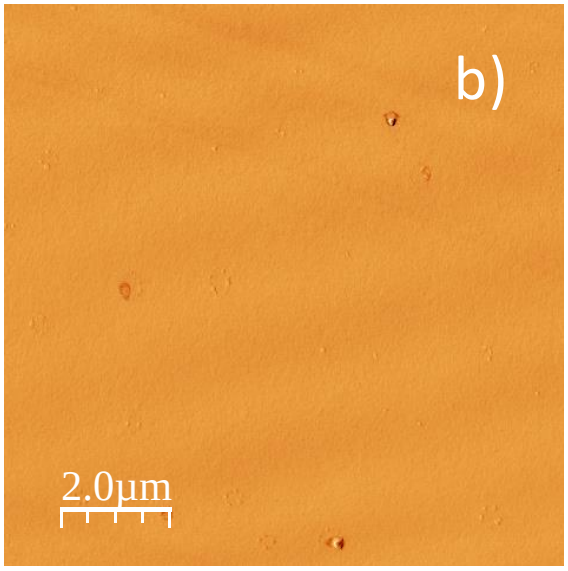

Figure 4. AFM surface morphologies of the sol-gel coating formed on the AZ31 (a) and AZ61 (b) alloys substrates

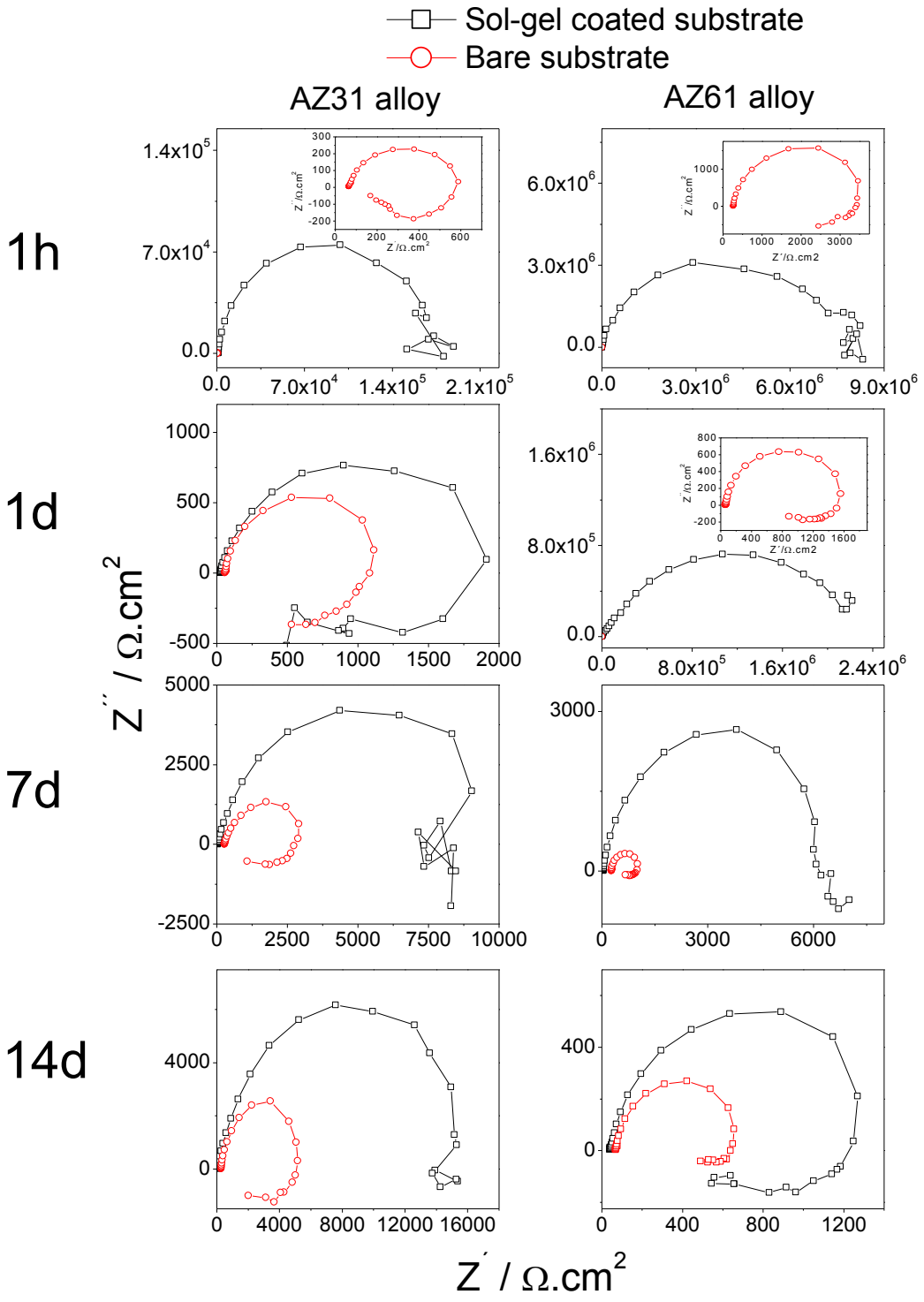

Figure 5. Variation in Nyquist plot as a function of the coated alloy type substrate over 14 days immersion in 0.6M NaCl solution

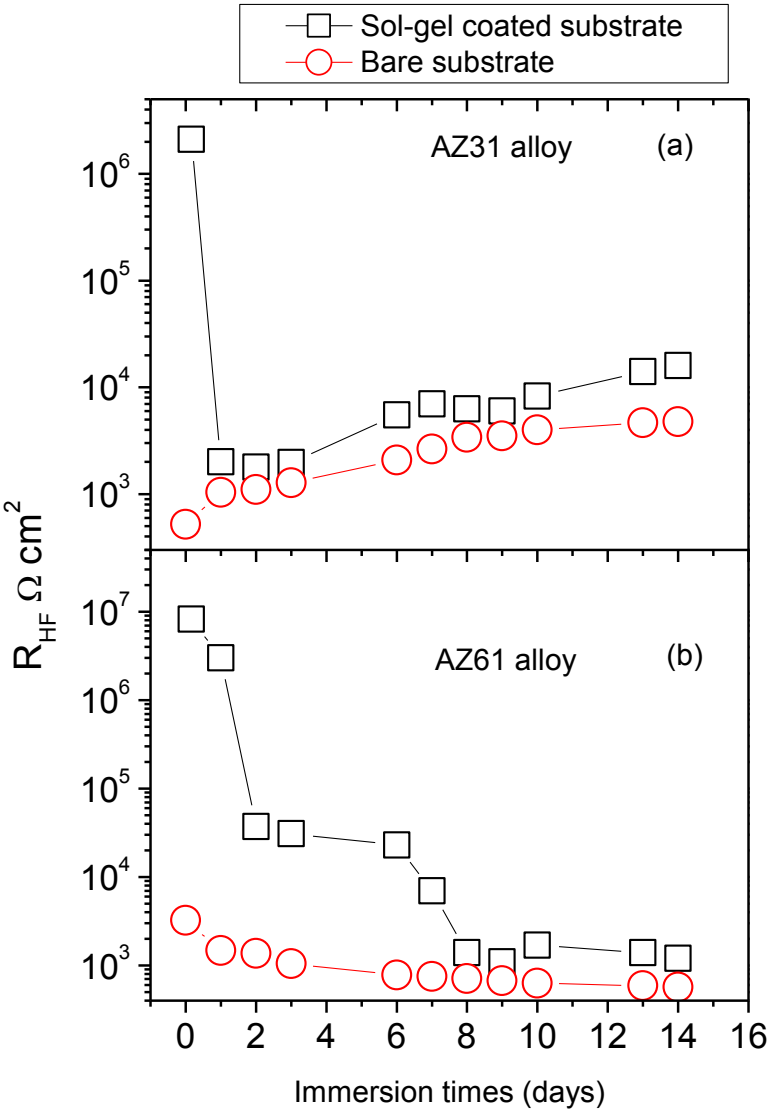

Figure 6. Variation in R_{HF} values as a function of the coated alloy type substrate over 14 days immersion in 0.6M NaCl solution

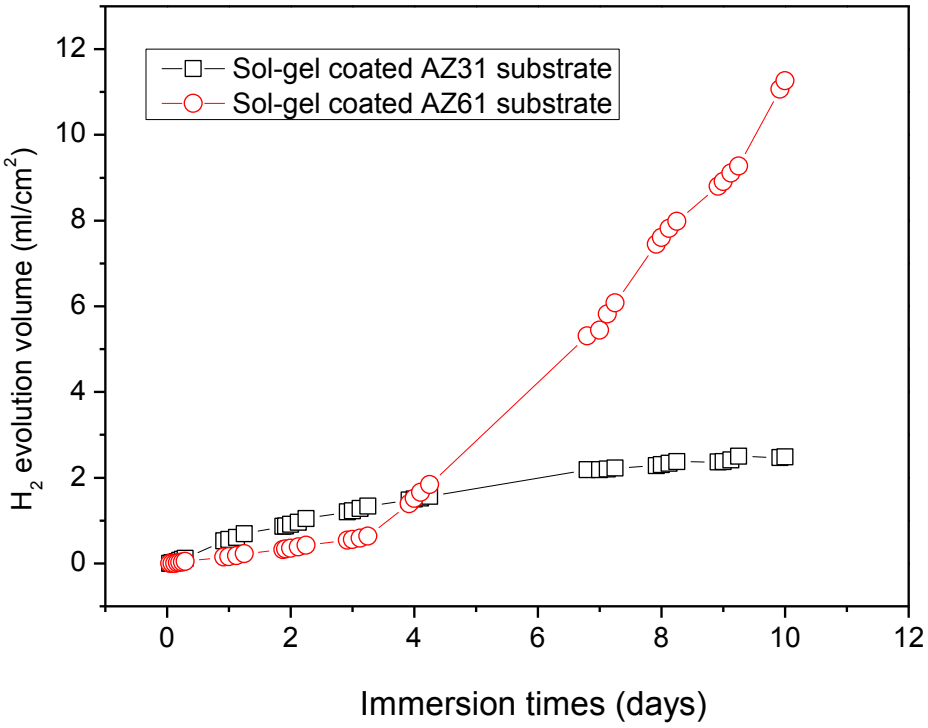

Figure 7. Hydrogen evolution curves as a function of the coated alloy type substrate over 11 days immersion in 0.6M NaCl solution

.

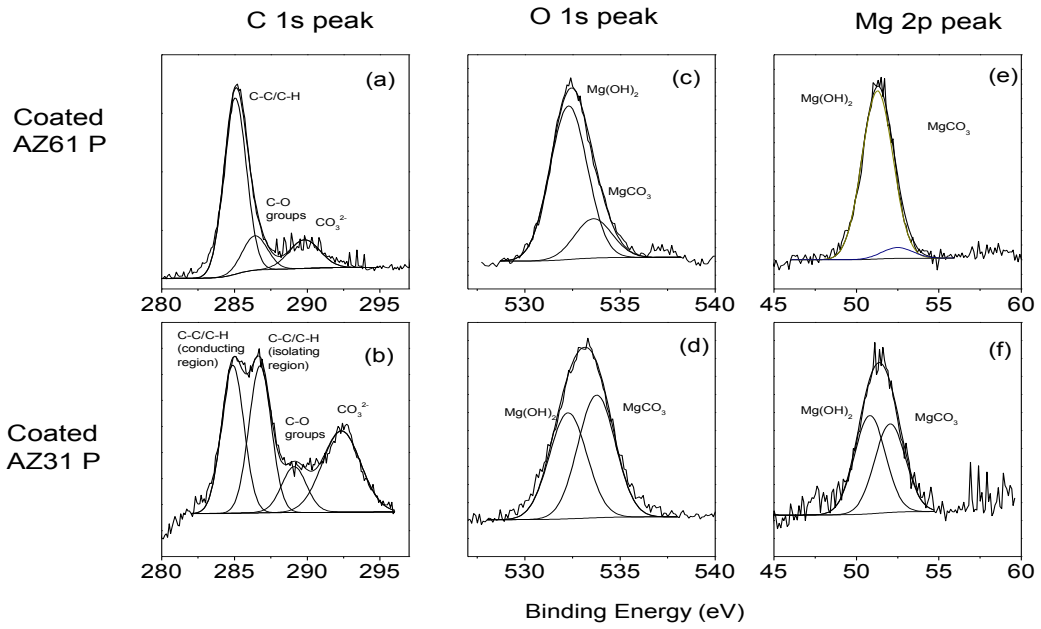

Figure 8. C1s, O1s and Mg2p high-resolution peak obtained by XPS on the surface of the sol-gel coated as a function of the type alloy substrate after 14 days immersion in 0.6M NaCl solution

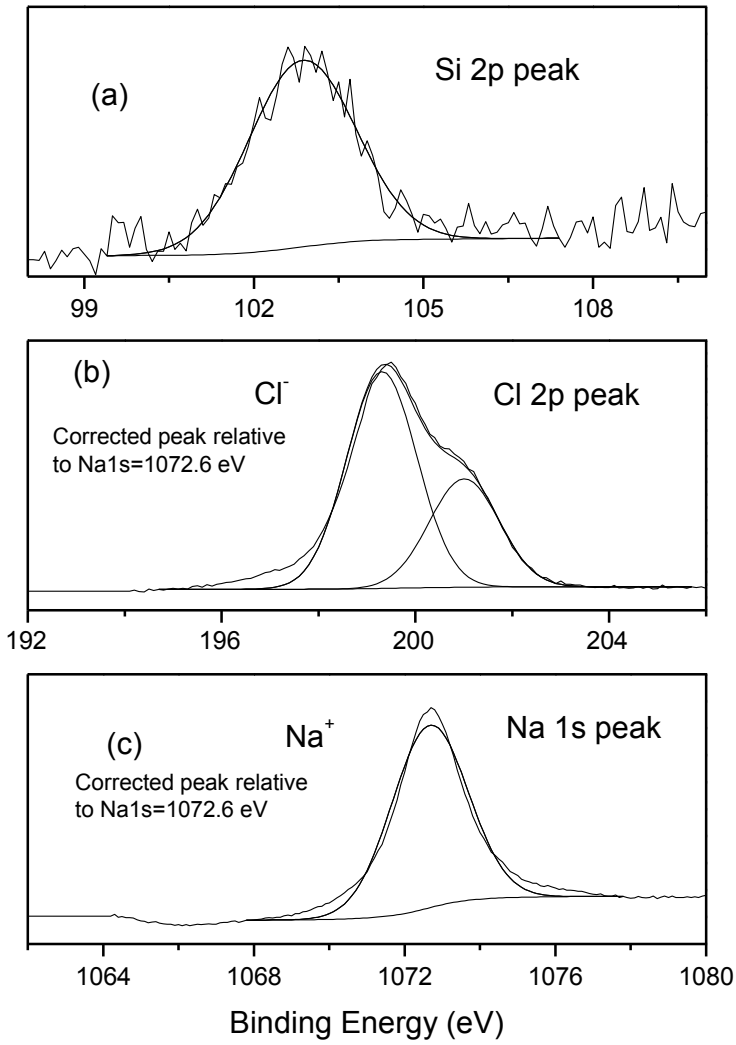

Figure 9. Si2p (a), Cl 2p (b) and Na1s (c) high resolution peak obtained by XPS on the surface of the sol-gel coated AZ31 alloy substrate after 14 days immersion in 0.6M NaCl solution

Table 1. Chemical composition of AZ31 and AZ61 alloys (wt. %)

Alloy	Al	Zn	Mn	Si	Fe	Ca	Mg
AZ31	3.1	0.73	0.25	0.02	0.005	0.0014	Bal.
AZ61	6.2	0.74	0.23	0.04	0.004	0.0013	Bal.

Table. 2 Assignment of the ATR bands in MAPTMS/TMOS coatings reported [12]

Wavenumber (cm^{-1})	**Group**	**Assignment**
2942	(C-H)s	Organic
1450	C–H	Organic
1750	C=O	Organic
893	(Si–O–Mg)	interface
1100	(Si–O–Si)	Inorganic Backbone
3436	Si-OH	

Table 3. Atomic percentage observed by XPS of the external surface of AZ31 and AZ61 coated with sol-gel

Alloy	%C	%O	%Si	% Mg
AZ31	16	53	29	2
AZ61	14	56	30	0

Table 4. Atomic percentage observed by XPS of the external surface of AZ31 and AZ61 coated with sol-gel after immersion for 15 days in 0.6 M NaCl solution.

Alloy	% C	%O	%Mg	%Al	%Si	%Cl	%Na[a]	CO_3^{2-} (obtained from the fitting of the C 1s peak and the C atomic percentage)	
AZ31	38	11	3	0	1	17	29	13	85
AZ61	39	31	11	0	0	10	11	6	48

[a] Approximate Na values including the contribution from Na1s peak (1071.6) and Cl kk auger peak after sum of signals from Na1s peak and ClKll auger carbon, oxygen and zinc.